Mechano-Stimulus and Environment Dependent Circularly Polarized TADF in Chiral Copper(I) Complexes and their Application in OLEDs

André Martin Thomas Muthig,[†] Ondřej Mrózek,[†] Thomas Ferschke,[‡] Maximilian Rödel, [‡] Björn Ewald, [‡] Julia Kuhnt,[†] Carsten Lenczyk,[†] Jens Pflaum,[‡,*] Andreas Steffen[†,*]

[†]Department of Chemistry and Chemical Biology, TU Dortmund University, Otto-Hahn-Str. 6, 44227 Dortmund, Germany.

[‡]Experimental Physics VI, Julius-Maximilian University, Am Hubland, 97074 Würzburg, Germany.

TADF, circularly polarized luminescence, OLED, copper, chiral complexes

ABSTRACT: Molecular emitters that combine circularly polarized luminescence (CPL) and high radiative rate constants of the triplet exciton decay are highly attractive for electroluminescent devices (OLEDs) or next generation photonic applications, such as spintronics, quantum computing, cryptography or sensors. However, the design of such emitters is a major challenge because the criteria for enhancing these two properties are mutually exclusive. In this contribution, we show that enantiomerically pure [Cu(Cbz^R)((*S*/*R*)-BINAP)] (R = H (**1**), 3,6-*t*Bu (**2**)) are efficient TADF emitters with high radiative rate constants of k_{TADF} up to $3.1 \cdot 10^5$ s^{-1}, and exceptional dissymmetry values of the emission g_{lum} of $\pm 0.7 \cdot 10^{-2}$ in THF solution and $\pm 2.3 \cdot 10^{-2}$ in the solid state are observed. Importantly for application in electroluminescence devices, the efficiency of the TADF process and emission wavelengths are highly sensitive to environmental hydrogen bonding of the ligands, which can be disrupted either by grinding of the crystalline materials or by employing sterically bulky matrices. Accordingly, we have investigated various matrix materials for successful implementation of the chiral copper(I) TADF emitters in proof-of-concept CP-OLEDs.

INTRODUCTION

The efficiency and further development of photonic applications such as OLEDs, data encryption, optical quantum technologies or quantum computing, would greatly benefit from the development of emitter materials that can exhibit circularly polarized luminescence (CPL).[1] Circular polarization (CP) of photons is analogous to the spin of electrons, with an associated spin angular momentum quantum number $J_z = \pm\hbar$, which translates into left- and right-handedness of the electromagnetic field due to a phase shift between the electronic and magnetic field vectors by $\pm\pi/2$.[2] Usually, molecular emitters generate light with linear polarization along the direction of the electronic transition dipole moment vector as their ensemble does not discriminate between photons of different J_z, i.e. in the collective, light particles are undefined with respect to their CP and interfere to give an "in-phase" electromagnetic wave.[3] With this background, various classes of molecular luminophores have been investigated to elucidate synthetic design criteria by following the idea, that the handedness of the emitted photons can be connected to the chirality of the emitter itself, which should provide a rotatory strength R for the electron density change during the transition from the excited to the ground state.[4,5] Thus, the radiative decay requires a maximized magnetic transition dipole moment vector $|\vec{m}|$ ideally aligned (anti-)parallel to the electronic transition dipole moment vector $|\vec{\mu}|$ for high dissymmetry factors g_{lum} according to Eq. 1.[5,6]

$$g_{lum} = \frac{4R}{|\vec{\mu}|^2+|\vec{m}|^2} = \frac{4|\vec{\mu}||\vec{m}|\cos\theta}{|\vec{\mu}|^2+|\vec{m}|^2} \quad \text{(Eq. 1)}$$

The g_{lum} represents the degree of CPL achieved by the luminophore, with the maximum values of ±2 describing emission of photons of solely right- or left-handedness. Bearing in mind that $|\vec{\mu}|$ is typically several orders of magnitude larger than $|\vec{m}|$,[7] the obvious drawback when achieving high g_{lum} values is the precondition that $|\vec{\mu}|$ must be relatively small, i.e. the emission process bears little oscillator strength and thus, as a side effect, small radiative rate constant k_r, which can be detrimental for the quantum yield ϕ.[8] It is important to note that high k_r are particularly important to minimize premature decomposition of the emitters and undesired charge built-up in electrically driven devices, where predominantly long-living triplet excitons are harvested for formally spin-forbidden emission.[9–11] In order to solve this dilemma, a fine balance between $|\vec{\mu}|$ and $|\vec{m}|$ for efficient and fast triplet exciton CPL must be adjusted.

Accordingly, transition metal complexes of, e.g., the 4d and 5d elements Ru^{II}, Ir^{III} and Pt^{II} as prototypical OLED emitters have been studied with regard to their chiroptical properties, but the large majority showed low $g_{lum} < 3 \cdot 10^{-3}$.[12] An exception is a family of Pt^{II} complexes with chiral helicene-type ligands that can give respectable dissymmetry values of $1.3 \cdot 10^{-2}$ originating from the molecular properties,[13] while aggregation and formation of chiral assemblies led to exceptionally high $g_{lum} = -6.4 \cdot 10^{-2}$ for **A** as reported by Park et al. (Scheme 1).[14] Significantly larger dissymmetry values can be obtained from metal-centered (MC) states that are Laporte-forbidden, such as in chiral Cr^{III} spin-flip complexes. Piguet et al. reported record g_{lum} of ±0.2 for **B**,[15] and also Heinze and co-workers demonstrated that the concept of μ-forbidden/m-allowed MC transitions

works in **C** with a value of ±0.1.[16] However, these formidable values come at the price of low $k_r < 10^3$ s^{-1} similar to those of electronic dipole forbidden f-f transitions in lanthanide complexes, seriously limiting the value of these classes of chiral emitters for application in devices.[9–11] Reports on molecular chiral emitters based on 3d transition metals are generally scarce, but a series of menthone derived [CuX(CAAC)] (X = halides, F (**D**), Cl (**E**), Br (**F**), I (**G**); CAAC = cyclic (alkyl)(amino)carbene) complexes has been reported to exhibit low $g_{lum} = \pm 1 \cdot 10^{-3}$.[17] Some chiral aggregates and Cu^{I} clusters have been found to reach relatively high dissymmetry values of up to $\pm 2 \cdot 10^{-2}$, but such compounds are difficult to process for applications.[18]

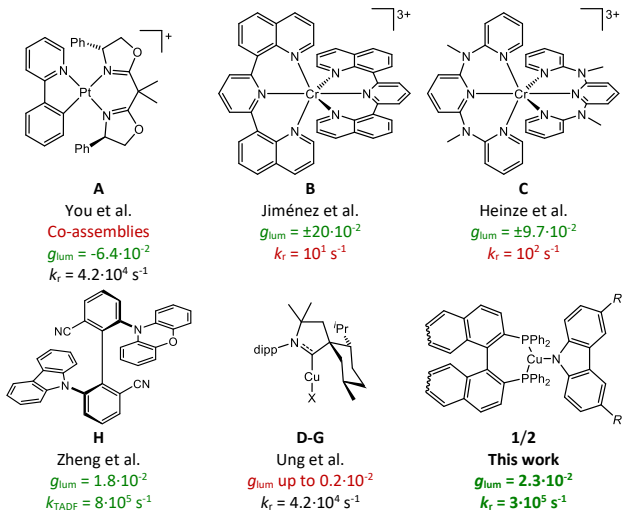

Scheme 1. Comparison of selected classes of chiral emitters with regard to their luminescence dissymmetry factors g_{lum} and radiative rate constants k_r of triplet exciton emission.

A different approach is to employ chiral thermally activated delayed fluorescence (TADF) emitters that bypass the spin-forbidden phosphorescence from T_1 by reverse intersystem-crossing (rISC) and radiative decay from the S_1 state, of which the small $|\vec{\mu}|$ necessary for CPL properties would still provide a high k_r of triplet exciton emission due to the spin-allowed nature of the transition $S_1 \rightarrow S_0$. Various organic intrinsically chiral TADF emitters have been studied in the past decade, in which the dissymmetry is induced either by chiral moieties such as the [2.2]paracyclophane motif[19] or by axial chirality. Although the axially chiral **H** BPPOACz described by Tu et al. gave remarkable $g_{lum} = 1.8 \cdot 10^{-2}$, the vast majority of organic TADF compounds remained at $< 3 \cdot 10^{-3}$.[20]

Interestingly, transition metal derived TADF emitters that add spin-orbit coupling (SOC), which can also influence $|\vec{\mu}|$ and $|\vec{m}|$, have not yet been studied with regard to their CPL properties. As part of our long-standing interest in developing structure-property relationships for efficient Cu^{I}-based triplet and TADF emitters,[21] we have now embarked on investigating the influence of chiral ligand frameworks on the dissymmetry of their electronic vertical transitions and application thereof. Specifically, we herein report on the design of enantiomerically pure copper(I) TADF complexes by employing (*S*/*R*)-BINAP as an acceptor unit and a carbazolate (Cbz) ligand as a donor to access chiral ligand-to-ligand charge-transfer (LLCT) states, that also benefit from the SOC of the metal center by additional metal-to-ligand (ML)CT states. The TADF process of the resulting compounds can reach k_r of up to $3 \cdot 10^5$ s^{-1}, but is highly dependent on the environment with respect to emission wavelength λ_{em} and k_r, which we attribute to specific C–H···π interactions with neighboring matrix molecules that can be disrupted by grinding of the single crystals, leading to pronounced mechanochromic luminescence. Similar effects have previously been described for other organometallic TADF emitters, but mostly related to intramolecular geometrical changes.[22] In our case, the mechanism is significantly different and relevant for device applications, as we demonstrate that using bulky or unpolar matrix materials incapable of undergoing hydrogen bonding has an enormous influence on the TADF performance. The chiral structural motif indeed leads to high dissymmetry factors g_{lum} of up to $\pm 7 \cdot 10^{-3}$ in THF solution and $\pm 2.3 \cdot 10^{-2}$ in the solid state, and in combination with the high k_r, this new class of CP-TADF compounds has been applied in CP-OLEDs.

RESULTS AND DISCUSSION

Synthesis and Structural Characterization. The chiral copper(I) complexes **(*S*/*R*)-1** and **(*S*/*R*)-2** have been prepared by addition of (*S*)- or (*R*)-BINAP, respectively, to a suspension of CuCl in THF and subsequent reaction of the intermediary chloride complexes with KCbz^{R} (Cbz = carbazolate, R = H, *t*Bu) (Scheme 2). The products were finally collected as yellow crystalline materials in good to excellent yields of 41-86% by slow diffusion of cyclohexane and *n*-pentane into saturated solutions of either tetrahydrofuran (THF) or dichloromethane (see ESI). The structures of compounds **(*S*/*R*)-1** and **(*S*/*R*)-2** obtained by single-crystal X-ray diffraction studies are shown in Figure 1.

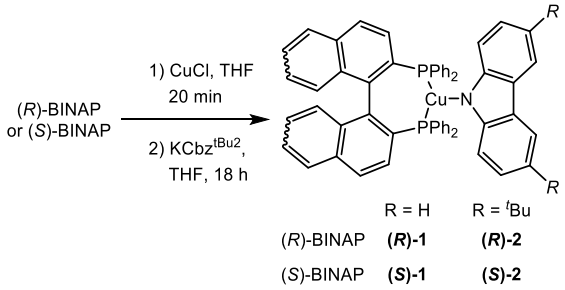

Scheme 2. Synthesis of enantiomerically pure [Cu(Cbz^{R})((*S*/*R*)-BINAP)] (R = H (1), *t*Bu (2)).

Despite the trigonal coordination geometry, the Cu–P bond lengths of the respective compounds are not identical and deviate by ca. 0.015-0.019 Å, a phenomenon that has also been observed in trigonal [Cu(Cbz)(PPh$_3$)$_2$] (0.030 Å), tetrahedral [Cu(BF$_4$)(3,5-dimethylpyrazole)(BINAP)] (0.274 Å) and dimeric {CuCl(BINAP)}$_2$ (0.005 Å).[23,24] For **(*S*/*R*)-1** and **(*S*/*R*)-2**, this might partly be due to packing effects in the solid state, as the DFT geometry optimized structure has nearly identical Cu–P bonds (Tables S15 and S17). The BINAP complexes **(*S*/*R*)-1** and **(*S*/*R*)-2** exhibit shorter Cu–N(Cbz) bonds of 1.919(2)-1.917(2) Å and slightly smaller differences of the N-Cu-P(1/2) angles of 0.5° and 3.0°, respectively, in comparison to [Cu(Cbz)(PPh$_3$)$_2$] with 1.9499(11) Å and 5.7°. However, the dihedral angle between the Cbz ligand and the plane defined by the metal center and the P atoms is only 26-29° for **(*S*/*R*)-1** and **(*S*/*R*)-2**, whereas [Cu(Cbz)(PPh$_3$)$_2$] is much more distorted with ca. 41°. It is important to note that C–H···π interactions between

the BINAP and the Cbz ligands of the surrounding complex molecules occur in the single crystalline solid state, which stabilizes the ground state, but would destabilize CT states that experience a different electron density distribution (vide infra).

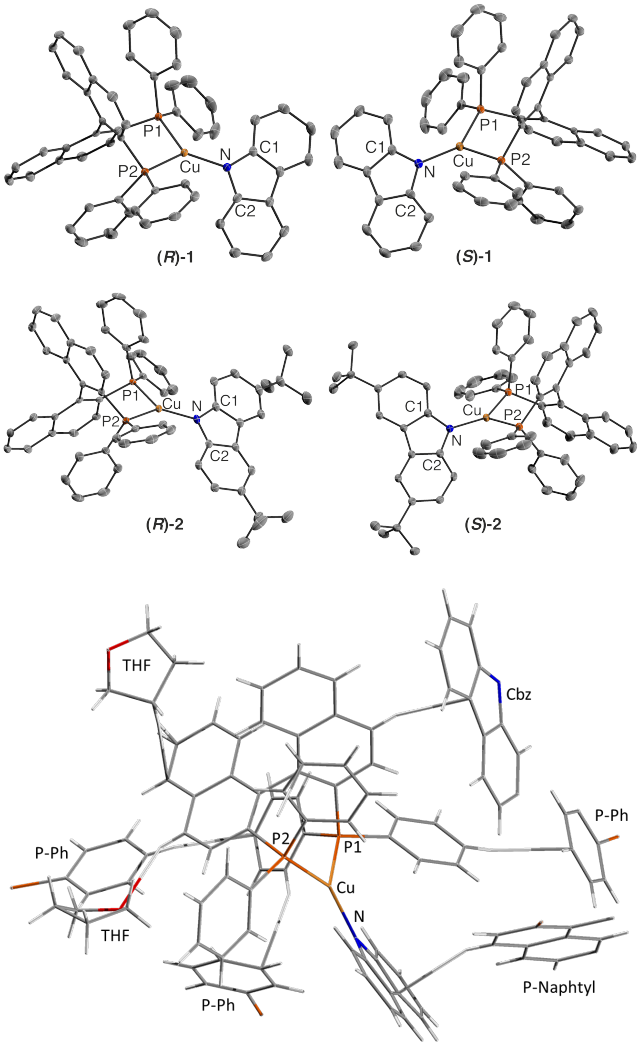

Figure 1. Molecular structures of **(*S/R*)-1** and **(*S/R*)-2** in the single crystalline solid state (top) and hydrogen bonding with neighbor molecules in the unit cell (bottom). Thermal ellipsoids were drawn at the 50% probability level; H atoms have been omitted for clarity. Selected bond lengths (Å) and angles [deg] for **(*R*)-1**: Cu–P(1) 2.2430(8), Cu–P(2) 2.2577(9), Cu–N 1.919(2), P(1)–Cu–P(2) 101.09(3), N–Cu–P(1) 128.95(7), N–Cu–P(2) 129.51(7), dihedral Cbz–(P(1)CuP(2)) 29.15(10); **(*R*)-2**: Cu–P(1) 2.2519(8), Cu–P(2) 2.2711(8), Cu–N 1.917(2), P(1)–Cu–P(2) 98.85(3), N–Cu–P(1) 132.00(8), N–Cu–P(2) 129.00(8), dihedral Cbz-(P(1)CuP(2)) 26.34(18).

Electrochemical and Photophysical Studies in THF solution. For the following discussions we refer to the respective enantiomers only for chiroptical measurements, as all other properties are identical for the enantiomers of **1** and **2**. The copper(I) complexes **1** and **2** show Cbz ligand dependent, quasi-reversible oxidation potentials of 0.64 and 0.46 V vs. Fc^{+}/Fc, respectively, which is also nicely displayed in the difference of DFT calculated HOMO energies (-4.60 (**1**) vs. -4.47 (**2**) eV, see Figure S12 and Table S19). An irreversible reduction at ca. -2.0 V is observed for both, in line with the calculated very similar energies of the LUMO of -1.89 (**1**) and -1.90 (**2**) eV, that is primarily located at the BINAP ligand. These findings suggest that the low energy transitions of photoexcitation should be dominated by LLCT contributions (vide infra).

The UV-vis absorption in THF solutions of the Cu^{I} BINAP complexes **1** and **2** are very similar and can be divided in four major bands (**Figure 2**). Very broad low energy absorptions between λ_{abs} = 400-500 nm with small extinction coefficients of ε = ~1,000 $M^{-1}cm^{-1}$ indicative for orbital overlap and symmetry forbidden transitions arise from excitation to LL(Cbz→BINAP)CT states with ML(Cu→BINAP)CT admixtures according to our TD-DFT calculations (**Figure 3**). The absorption band λ_{abs} = 350-400 nm (ε = ~4,000 (**1**) and 6,500 (**2**) $M^{-1}cm^{-1}$) is due to transitions of dominantly ML(Cu→BINAP)CT character, while the much higher absorptivity between 320-400 nm results from LC states of the Cbz ligands, which contain some MLCT admixture according to the electron density difference representation of the $S_0 \rightarrow S_{15}$ transition of **(*S*)-1** (Figure 3). High energy absorptions beyond 320 nm with ε = 40,000-50,000 $M^{-1}cm^{-1}$ can be assigned to LC(π-π^*) transitions of the PPh_2 and naphthyl moieties.

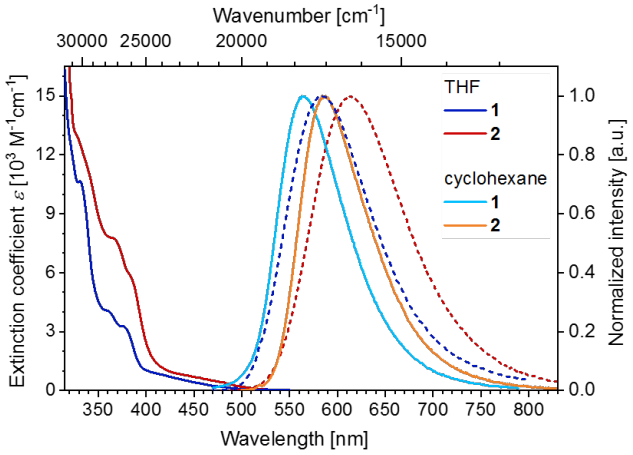

Figure 2. Absorption spectra in THF solution (dark solid), and emission spectra of [Cu(Cbz)(BINAP)] (**1**) and [Cu(Cbz$^{t\mathrm{Bu}}$)(BINAP)] (**2**) in THF (dark dashed) and cyclohexane solution (bright solid) at room temperature.

The emission of [Cu(Cbz)(BINAP)] (**1**) in THF solution is very broad with a maximum at λ_{em} = 585 nm and occurs with a rather short average lifetime of τ_{av} = 190 ns due to efficient non-radiative decay as evidenced by the low quantum yield ϕ < 0.013 (Figure 2 and **Table 1**). The data suggest a maximum radiative rate constant of $k_r = 6.8 \cdot 10^4$ s^{-1}, indicating that moderately efficient TADF from $^{1/3}$LLCT states is involved. Consequently, solvents of lower polarity, such as toluene or cyclohexane, give rise to hypsochromic shifts to λ_{em} = 577 and 565 nm, respectively.

The electron donating *t*Bu substituents at the Cbz ligand in **2** lead to bathochromic shifts of the emission maxima to 614 and 586 nm in THF and cyclohexane, respectively, and simultaneously increase the rigidity and steric hindrance of the complex, which greatly enhances the luminescence efficiencies to ϕ =

0.17 and 0.22 (Table 1). This is quite surprising, as the energy gap law (EGL) typically dictates that lowering the emission energy of a given system decreases the luminescence efficiency.[25] However, the values of k_r = 2.3·10^5 (THF) and 1.9·10^5 s^{-1} (Cy) of **2** are greatly increased by factors of 3.4/2.4 in comparison to **1**, which seems to be sufficient to counteract the EGL. We attribute the origin of this counterintuitive behavior to an enhanced efficiency of the TADF mechanism in **2**. We note that the excitation spectra generally match the low energy region of the absorption spectra, and thus aggregation effects that might influence the emission can be excluded as an alternative explanation.

It is imperative to compare the photophysical properties of **1** and **2** with structurally related [Cu(Cbz)(PPh$_3$)$_2$] reported by Peters et al., that shows blue (λ_{max} = 461 nm) phosphorescence with ϕ = 0.24 in methylcyclohexane, indicating a low k_r of 2·10^4 s^{-1}.[24] It appears that the BINAP ligand is more beneficial for low energy LLCT/MLCT states and smaller $\Delta E(S_1\text{-}T_1)$ to allow for higher k_r, either by more efficient coupling with S_n states to borrow oscillator strength or via TADF.

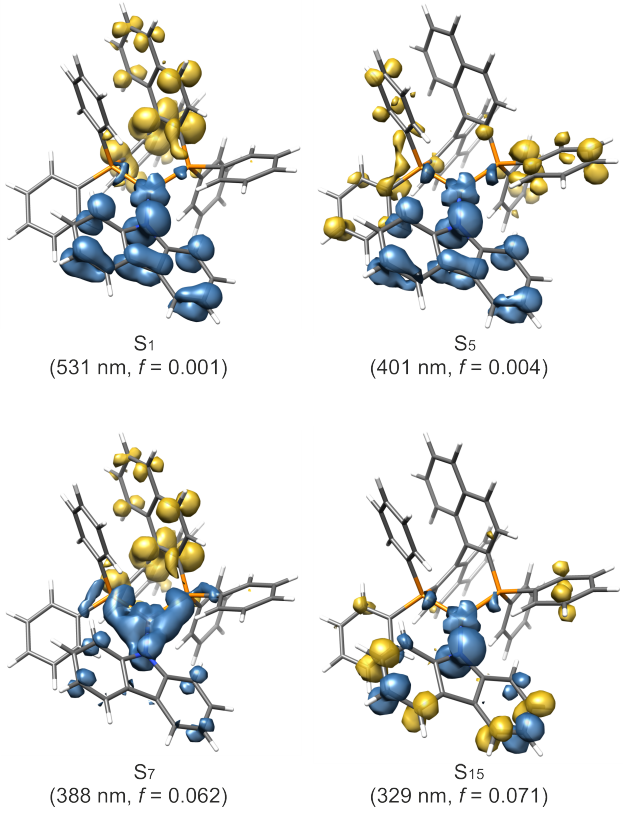

Figure 3. Differences between the electron density distributions of selected excited states and the electronic ground state S_0 of [Cu(Cbz)((*S*)-BINAP)] (**(*S*)-1**) relevant for the absorption spectrum in THF calculated at the D3(BJ)-PBE0/ZORA/def2-SVP level of theory. Loss of electron density is indicated in blue and gain in yellow (see also ESI).

Interestingly, steady-state and time-resolved luminescence measurements of [Cu(Cbz^{tBu})(BINAP)] (**2**) in frozen 2-MeTHF at 77 K show an enormous hypsochromic shift from $^{1/3}$LLCT states towards a vibrationally resolved, localized ^{3}BINAP state with millisecond lifetimes (Figure S9 and Table 1). This behavior can be explained as follows. As reported for some other d^{10} coinage metal complexes with a donor-M-acceptor structure,[26,27] the ground state of our copper(I) complexes is more polar than the excited state ($\Delta\mu_{calc}$= +10.1 D (**1**), +7.8 D (**2**)). Upon photoexcitation in solution at room temperature, the surrounding solvent molecules can rearrange their orientation in response to the changed electron density distribution in the excited state of the Cu^I compounds, which leads to stabilization of the CT state and simultaneous destabilization of the ground state at that particular geometry. However, in a frozen matrix the solvent molecules cannot reorientate freely to acknowledge the new dipole interactions in the excited state of the copper(I) complex, which destabilizes the $^{1/3}$LLCT states and the system is trapped in a high energy ^{3}LC at the BINAP.

Photocatalytic properties of [Cu(Cbz^{tBu})(BINAP) (2). In order to further prove the formation of triplet states upon photoexcitation in solution, we investigated the energy transfer properties of compound **2** within the *trans*-/*cis*-isomerization of stilbene, which is known to occur via population of its ^{3}(π-π*) state.[28] Indeed, *cis*-stilbene is formed in 85% yield within 4 hours when **2** is added in 3 mol-% under 475 nm light irradiation (**Figure 4** and S11). The luminescence quenching experiments reveal a dynamic process, i.e. Dexter energy transfer from the T_1 state of **2** and not static quenching by aggregation of stilbene and the copper(I) complex in its ground state. Interestingly, the Stern-Volmer constant K_{SV} of 30 M^{-1} yields a low bimolecular quenching constant $k_q = K_{SV}/\tau_0$ = 7·10^6 M^{-1}s^{-1} and points to an inefficient, non-diffusion-controlled process. Apparently, the steric hindrance in **2** antagonizes the prerequisite of good orbital overlap between donor and acceptor for efficient Dexter energy transfer. This finding is also in line with the higher ϕ for photoluminescence of **2** found in THF solution in comparison to **1** (vide supra).

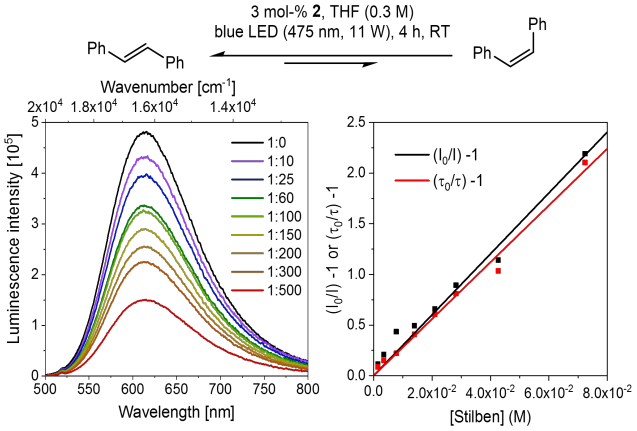

Figure 4. Photocatalytic *trans*-/*cis*-isomerization of stilbene by **2** upon irradiation at 475 nm (top). Luminescence quenching of **2** in the presence of varying amounts of stilbene (left) and corresponding Stern-Volmer plot (right). For further details, see ESI.

Table 1. Photophysis of 1 and 2 in Solution, Microcrystalline, Ground Solid State, and various OLED Matrices under Argon.

	medium	T [K]	λ_{em}[a] [nm]	τ [µs][b]	τ_{av} [µs]	ϕ	k_r [10^4 s^{-1}][c]	k_{nr} [10^4 s^{-1}][c]
1	THF	295	585	0.17 (96), 0.68 (4)	0.19	0.013[e]	6.8	520
	toluene	295	577	0.12 (97), 0.57 (3)	0.13	-		
	cyclohex-ane	295	565	0.31 (96), 2.8 (3), 13.2 (1)	0.51	0.04	7.8	190
	crystalline	295	564	5.0 (91), 46.0 (9)	8.7	0.25	2.9	8.7
	ground	295	579	2.1 (94), 9.0 (6)	2.5	0.55	22	18
		77	580	105 (38), 480 (44), 1466 (18)	515	0.74	0.14	0.05
		17	577	223 (43), 840 (46), 2421 (11)	749			
	mCP (1)	295	534	5.7 (78), 22.9 (19), 184 (3)	14.3	0.64	4.5	2.5
	CzSi (10)	295	575	1.7 (76), 3.7 (24)	2.2	0.47	21	24
	UGH-3 (10)	295	575	2.1 (91), 5.4 (9)	2.4	0.30	13	30
	PMMA (1)	295	553	6.7 (72), 19.5 (25), 75.8 (3)	12.0	0.47	3.9	4.4
		77	551	461 (39), 1404 (49), 3616 (12)	1302	0.47	0.036	0.04
		7	551	282 (31), 1231 (51), 3555 (18)	1355			
2	THF	295	614	0.73		0.17	23	112
		77	498	2400 (39), 6100 (61)	4657	n.d.		
	cyclohex-ane	295	586	1.2		0.22	19	67
	crystalline	295	549	19.2 (74), 62.6 (26)	30.5	0.22	0.72	2.6
		77	538	557 (57), 1652 (43)	1028	0.08	0.008	0.09
		5.3	498	2400 (47), 8252 (48), 23901 (5)	6284	n.d.		
	ground	295	606	1.4 (94), 6.6 (6)	1.7	0.53	31	27
		77	603	68.7 (58), 446 (42)	227	0.25	0.11	0.33
		5.8	601	239 (47), 1038 (43), 2817 (10)	840	n.d.		
	mCP (1)	295	538	4.6 (75), 24.4 (21), 157 (4)	149	0.51	0.34	0.33
	CzSi (10)	295	595	0.96 (70), 2.0 (30)	1.3	0.14	11	68
	UGH-3 (10)	295	590	0.83 (71), 2.0 (29)	1.2	0.18	15	68
	PMMA (1)	295	540	50.3 (86), 519 (14)	116	0.46	0.40	0.47

[a]The respective maxima are given. [b]For biexponential decays, the pre-exponential factors are given in parentheses. [c]Estimated from $k_r = \phi/\tau$.

Mechanochromic Luminescence behavior in the solid state. The emission in the single-crystalline solid state is broad and hypsochromically shifted compared to polar THF solution to λ_{em} = 564 and 549 nm for **1** and **2**, respectively, with a much more pronounced effect for **2** (Figure 5 and Table 1). Due to increased rigidity, the quantum yields of ϕ = 0.22 (**1**) and 0.25 (**2**) are higher than in solution and the time-resolved photoluminescence (TRPL) decays are bi-exponential, providing averaged lifetimes of τ_{av} = 8.7 (**1**) and 30.5 (**2**) µs (Table 1). Interestingly, while the estimated k_r = $2.9 \cdot 10^4$ s^{-1} of [Cu(Cbz)(BINAP)] (**1**) is ca. half of the value obtained in solution, the *t*Bu derivative **2** experiences a more drastic decrease by nearly two orders of magnitude to $k_r = 0.7 \cdot 10^4$ s^{-1}. The long lifetimes in the millisecond regime and pronounced vibrational progression of the emission of [Cu(Cbz$^{t\text{Bu}}$)(BINAP)] (**2**) at low temperatures indicate thermal population of the ^{3}LLCT state from a ^{3}LC state of the BINAP (Figure 5). Although we cannot exclude a minor involvement of TADF via an additional $^{1/3}$LLCT equilibrium at 295 K, the low $k_{r,295K}$ of both **1** and **2** favor the interpretation of dominantly phosphorescence from ^{3}LLCT/BINAP states.

We rationalize the hypsochromic shift and lower k_r in the crystalline solid state as follows. The environment of the excited molecule consists of highly symmetrically surrounding polar copper(I) complex molecules that mainly remain in their ground state due to the relatively low extinction coefficients. The dense packing in the single crystals prohibits their reorientation to acknowledge the new dipole interactions in the excited state, resulting in a destabilization. In addition, X-ray diffraction studies show significant C–H$\cdots\pi$ interactions between the BINAP ligand and the PPh_2 and Cbz moieties of other complexes (Figure 1). Although this leads to a stabilizing effect in the ground state, the new electron density distribution in the excited state of LLCT character is further destabilized even into the energetic region of the ^{3}BINAP state, and thus a hypsochromic shift in emission is observed. The interactions in the crystalline solid state apparently also increase the energy gap between the $^{1/3}$LLCT states, so that TADF becomes very inefficient with a major phosphorescent component as described above.

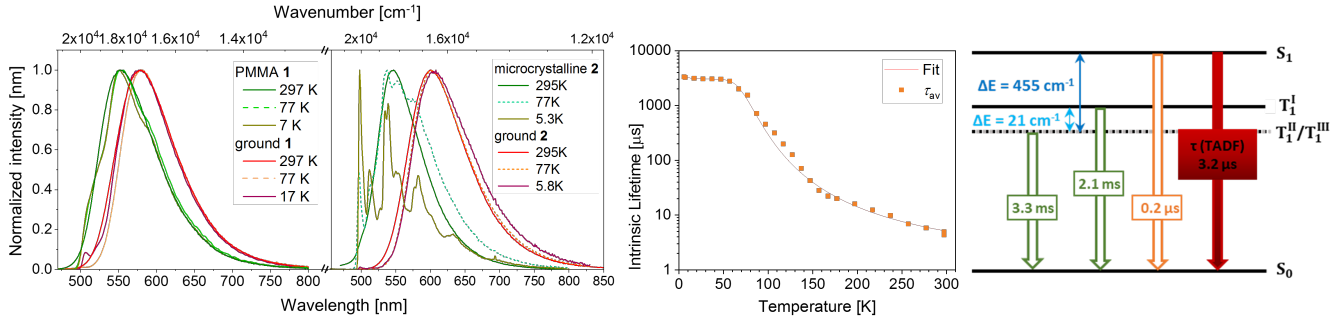

Figure 5. Left: temperature dependent emission spectra of **1** in PMMA and ground solid state, and of **2** in microcrystalline and ground state. Right: radiative lifetime of **2** in the ground solid state at various temperatures and state diagram visualizing the TADF process.

Upon grinding, the intermolecular C–H···π interactions are disrupted and the number of surface molecules of the microcrystals increases, reducing the effects of surrounding dipoles. Consequently, the broad CT emission of **1** and **2** is bathochromically shifted to 589 and 606 nm, respectively, with a concomitant drastic increase of k_r to $2.2 \cdot 10^5$ and $3.1 \cdot 10^5$ s^{-1}, respectively (Figure 5). Apparently, the smaller energy splitting between the $^{1/3}$LLCT states and their larger energetic separation from the ^{3}BINAP states allows a switch of emission mechanism to TADF. The fitting parameters obtained from the variable temperature measurements of **2** give $\Delta E(S_1\text{-}T_1)$ of 455 cm^{-1}, which nicely matches the shift of the experimental emission onset between the ^{1}LLCT at 295 K and the ^{3}LLCT state at 5.8 K.

Matrix dependent TADF properties. With the indication of specific environment interactions being potentially decisive for the TADF properties of the BINAP complexes **1** and **2**, we investigated their photophysics in various matrices relevant for device applications (Table 1, and Figure 6 and S7-S9).

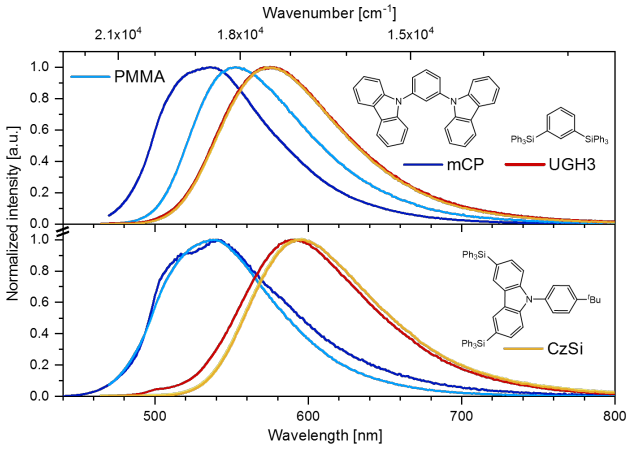

Figure 6. Emission spectra of [Cu(Cbz)(BINAP)] (**1**) and [Cu(Cbz$^{t\text{Bu}}$)(BINAP)] (**2**) in various matrices relevant for device applications and structures thereof.

In unpolar 1,3-bis(triphenylsilyl)benzene (UGH-3), no significant dipole interactions are expected and, consequently, low energy emission at λ_{max} = 575 (**1**) and 590 (**2**) nm similar to the ground solid state or in unpolar solvents is found with k_r of $1.3 \cdot 10^5$ (**1**) and $1.5 \cdot 10^5$ s^{-1} (**2**) showing an efficient TADF process. In contrast, highly polar matrices such as 1,3-bis(N-carbazolyl)benzene (mCP) or polymethylmethacrylate (PMMA) shift the emission hypsochromic even beyond the crystalline solid state and lower the k_r significantly by one to two orders of magnitude. Apparently, the efficiency of the TADF process is severely hampered due to an increased $\Delta E(S_1\text{-}T_1)$ and concomitant strong mixing with phosphorescence from ^{3}BINAP states (vide supra). At first glance, one would argue for destabilizing dipole-dipole interactions of the excited state of **1** and **2** with the surrounding rigid polar matrix being responsible for these photophysical changes as found for other coinage metal amides.[26,29] However, in polar but bulky 9-(4-*tert*-butylphenyl)-3,6-bis(triphenylsilyl)-9H-carbazole (CzSi), an efficient lower energy TADF similar to UGH-3 or the ground powder is observed, suggesting that the dominating factor for phosphorescence or TADF is the specific hydrogen bonding of the polar moieties surrounding the emitting molecule as observed in the single crystals, which is absent in CzSi due to the steric constraints.

Chiroptical properties. The enantiomerically pure complexes **(*S*/*R*)-1** and **(*S*/*R*)-2** show circular dichroism in the ground state with absorption dissymmetry factors g_{abs} of ±0.01 and ±0.005, respectively, for the lowest energy transitions in THF (Figure 7 and Table 2). The magnetic transition dipole moments $|\vec{m}|$ = 0.18 and 0.24 μ_B obtained by TD-DFT for the $S_0 \rightarrow S_1$ transition of **(*S*)-1** and **(*S*)-2**, respectively, are in the range of those found for similarly sized chiral metal complexes.[30] Interestingly, the angle θ between $\vec{m}$ and the electronic transition dipole moment $\vec{\mu}$ approaches 180°, resulting in relatively high calculated dissymmetries of $g_{abs,calc}$ up to -0.068 for **(*S*)-2**. The discrepancy with the experimental values might originate from the overlap of the more allowed $S_0 \rightarrow S_2$ absorption band, which exhibits a nearly parallel orientation of $\vec{m}$ and $\vec{\mu}$ with positive dissymmetry values, thus reducing the overall observed g_{abs} (Table 2). Although the radiative rate constants k_r of **1** and **2** suggest different relative efficiencies of the TADF process in THF solution (vide supra), their relatively high dissymmetry factors g_{lum} of ±0.007 (**(*S*/*R*)-1**) and ±0.006 (**(*S*/*R*)-2**) are very similar. The excited state distortion reduces the calculated dissymmetry of the emission in comparison to the calculated absorption, and is in line with the experimental values, but also enhances $\vec{\mu}$ by factors of ca. 6-28 leading to a beneficial combination of CPL and high oscillator strength (Table 2). We have estimated the radiative rate constant of CPL as a new measure of generated photon flux with the desired quantum property to $k_{CPL} = k_r \cdot g_{lum}/2 > 600$ s^{-1}, and an attractive CPL

brightness of $B_{CPL} \approx 2\ M^{-1}cm^{-1}$, which is in the range of the most efficient molecular chiral emitters featuring high k_r (for details, see ESI). Interestingly, the rigidity of the ground solid state, the environment where our Cu^I BINAP complexes exhibit the highest k_r ($2\text{-}3 \cdot 10^5\ s^{-1}$) of all studied matrices, even increases the degree of CPL to excellent values of $g_{lum} = \pm 0.023$ for **(*S*)-1**/**(*R*)-2**. To the best of our knowledge, these are the highest dissymmetry factors obtained for TADF emitters so far.

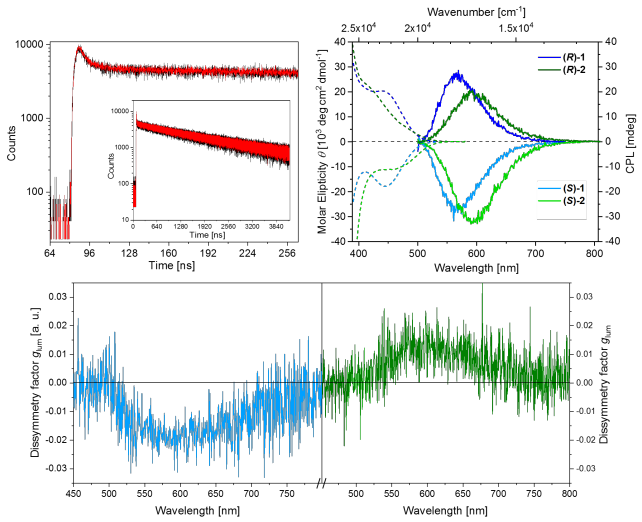

Figure 7. Top left: time-resolved polarization dependent photoluminescence decay of **(*S*)-1** in the ground solid state. Top right: circular dichroism (dotted) and circularly polarized luminescence (solid) of enantiomerically pure **(*S*/*R*)-1** and **(*S*/*R*)-2** in THF. Bottom: CPL of **(*S*)-1** (left) and **(*R*)-2** (right) in the ground solid state.

Table 2. Selected chiroptical properties of enantiomerically pure (*S*/*R*)-1 and (*S*/*R*)-2.

	g_{abs} [10^{-3}][a]	$\lvert\vec{m}\rvert$ [μ_B]	$\lvert\vec{\mu}\rvert$ [D]	θ [°]	g_{lum} [10^{-3}][b]
(*S*)-1 (exp.)	-10				-7
$S_0 \rightarrow S_1$ (531 nm)	-27	0.24	0.33	178	
$S_0 \rightarrow S_2$ (499 nm)	9.4	0.15	0.58	12	
$S_0 \rightarrow S_1$ (628 nm, T_1)	-7.5	0.42	2.1	173	
(*R*)-1 (exp.)	10				7
(*S*)-2 (exp.)	-5				-6 / -23[c]
$S_0 \rightarrow S_1$ (581 nm)	-68	0.18	0.10	180	
$S_0 \rightarrow S_2$ (544 nm)	6.7	0.09	0.49	12	
$S_0 \rightarrow S_1$ (686 nm, T_1)	-4.6	0.35	2.8	180	
(*R*)-2 (exp.)	5				6 / 23[c]

The difference in intensity along the various polarization directions raises the question on the underlying photophysical process governing excitation emission and their spatially anisotropic dynamics and transition rates. For this purpose, the time dependent intensity decay has been analyzed on various scales as function of direction of polarization. Representatively, Figure 7 shows the photoluminescence decay of compound **(*S*)-1** measured by time-correlated single photon counting (TCSPC) on thin films. Despite the fact that the overall intensity is different along different spatial directions by a factor of 1.18, and shows the angular variation as expected for CPL materials, the photophysical dynamics along diagonally oriented polarization axes, here 0 ° and 315 °, turned out to be identical. This holds true for short time-scales of nanoseconds (Figure 7, inset of top left), where the decay dynamics are determined mainly by direct fluorescence contribution to the intensity, but also for longer times of microseconds, where phosphorescent transitions and the reverse-intersystem crossing defines the emission of the compounds. As such, these data indicate and corroborate that the material inherent mechanisms of excitation and emission can be coherently described within a model based on just one set of transition rates without need to account for any specific directional variations, and that the S_1 and T_1 states both exhibit the same dissymmetry.

Implementation of [Cu(Cbz)(BINAP)] (1) in OLEDs. We have prepared proof-of-concept organic light emitting diodes (Figure 8 and Figure S13) employing **(*S*)-1** as active emitter in different matrices with varying polarity and steric complexity, namely mCP, 2,2',2"-(1,3,5-benzinetriyl)-tris(1-phenyl-1-H-benzimidazole) (TPBi) and CzSi. For mCP and TPBi matrix based devices, the electroluminescence maximum of **(*S*)-1** is observed at 545 nm, whereas it is bathocromically shifted by about 11 nm for the devices employing CzSi as host material (Figure 8). We attribute this shift to differences in specific C–H···π interactions between the matrix molecules and **(*S*)-1** affecting the energetic landscape experienced by the relevant contributing excited states and their dynamics as observed and rationalized for the photoluminescence properties, already. This bathochromic shift in the electroluminescence of **(*S*)-1**-doped CzSi devices is in qualitative agreement with the photoluminescence data discussed above, hinting again to the significant impact of C-H···π interactions on the radiative transitions extending to electrically driven devices. It has to be noted, however, that its magnitude as well as the absolute position of the emission maxima differ slightly. We attribute these observations to either an additional state admixture enrolled in the emission or to the presence of non-recombined charges yielding additional polarity contributions by the local environment in case of electrical operation.

Observation of circular dissymmetry in solid state light emitting devices is a highly pursued objective but turns out challenging due to, e.g., reflection at the metallic back electrode which is a key element in standard OLED design. Considering the situation of statistically positioned molecules within the device, emitting light of equal intensity in all directions (Lambertian emitter), in particular, towards the front glass support as well as the reflective back electrode. The CPL hitting the metal back electrode experiences a phase jump by π, effectively reversing its handedness and resulting in a superimposition of backward reflected and forward emitted light. Under idealized conditions of a back electrode with perfect (100 %) reflectance, the phase jump together with the intensity of the back reflected light would nullify the dissymmetry of the outcoupled polarized emission components.[31,32]

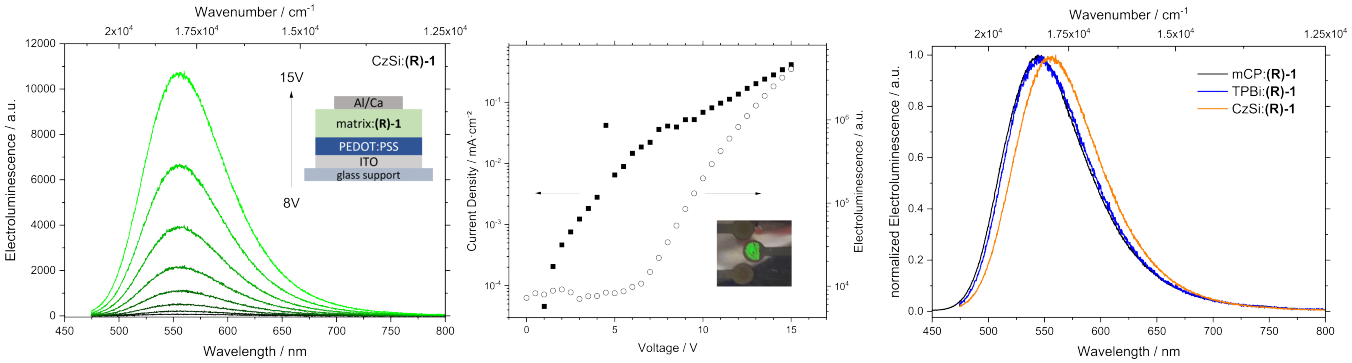

Figure 8. Left: general OLED stack architecture and electroluminescence spectra employing **(*S*)-1** as active emitter and CzSi as matrix. Middle: electronic characteristics of a CzSi: **(*S*)-1** OLED as function of forward voltage, and photograph of the electroluminescent diode. All devices exhibit an onset of electroluminescence at around 5±1 V. Right: normalized intensity measured under electrical operation of the OLED stacks for **(*S*)-1** doped into three different host matrices.

But since for real OLED device stacks the intensities of the superimposed spectral components are expected to be not exactly the same, residual dissymmetries will evolve and can be identified in the corresponding CPL spectra. We have therefore analyzed all fabricated OLED devices with respect to their polarization dependent electroluminescence dissymmetry. Figure 9 shows the effective electroluminescence dissymmetry of the examined light-emitting devices for several consecutive measurement cycles (line color fades for subsequent measurements). Each cycle comprises a subsequent measurement of both, 0° and 45°, polarization components (cf ESI). For mCP as well as TPBi based OLEDs, we observe a positive dissymmetry under electrical operation even though effects by intensity fluctuation and device deterioration are superimposed and render the evaluation demanding. For devices comprising an **(*S*)-1** doped CzSi matrix, these detrimental effects appear to be significant with respect to the magnitude of the detected emission dissymmetry and, hence, preventing a clear verdict on possible circular polarization asymmetries.

In summary, we were able to show the successful implementation of **(*S*)-1** as emissive molecular dopant in prototypical light-emitting devices. Despite utilizing the most basic single layer OLED architecture without further optimization of the individual stack design in respect to stability or out-coupling efficiency of polarized light, the circular polarization dissymmetry could be clearly confirmed for mCP as well as TPBi matrix-based devices. In case of CzSi matrix OLEDs a clear statement on this property is veiled by the interference of parasitic effects that might be solved by more advanced device concepts. Approaches towards this direction have to address the operational device stability as well as the polarization selective out-coupling efficiency, in combination leading to an improved signal-to-noise ratio and, hence, to a distinct contrast in the dissymmetry measurements as elucidated by Zinna et al .[31,33] Despite its attractivity for synthetic chemists, physicists as well as device engineers, we want, in a constructive statement, raise awareness that the small polarization differences in the luminescence of many organic compounds which become even smaller in electrically driven OLEDs as function of the operational conditions (Figure S14) can substantially influence the circular dissymmetry of their spectral emission. Hence, reliable conclusions on this parameter require for thorough investigations of all relevant polarization components in a true one-shot experiment and for accounting both the instrumental response as well as possible intensity fluctuations if one intends to quantify the chiral dissymmetry of solid state OLEDs.

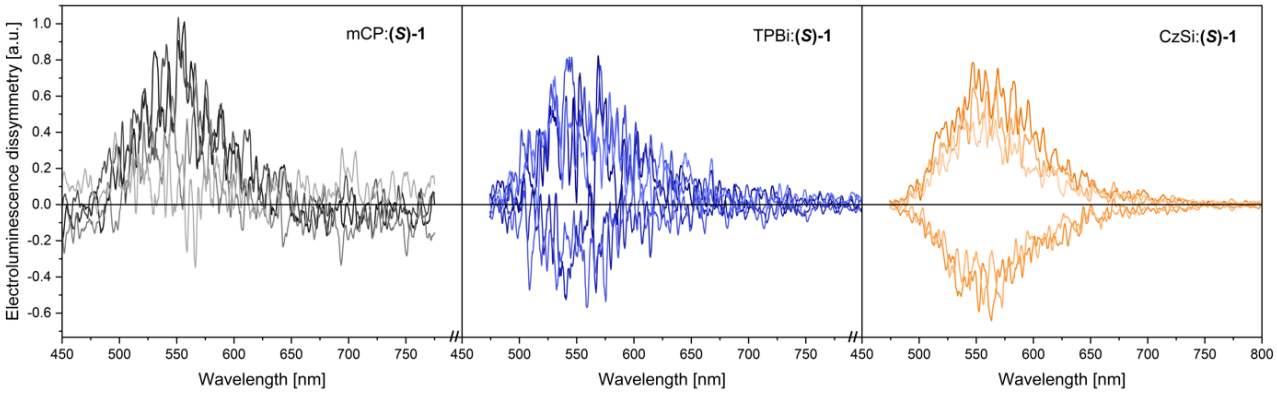

Figure 9. Spectrally resolved dissymmetry in the circular polarized electroluminescence of three different kinds of **(*S*)-1** doped OLEDs (line color fades for subsequent measurements). Whereas for OLEDs comprising a mCP and TPBi matrix, a positive dissymmetry can be identified in the measured CPL spectra (left and middle graph), a clear statement on this property in case of **(*S*)-1** doped CzSi devices is not feasible due to the significant impact of intensity fluctuations as well as deterioration of the devices during operation

CONCLUSIONS

We have reported the synthesis and structural characterization of enantiomerically pure trigonal coordinated [Cu(Cbz^R)((*S/R*)-BINAP)] (R = H (**1**) or 3,6-*t*Bu$_2$ (**2**)), which experience strong C–H···π interactions between the ligands and surrounding molecules, that greatly influence the photophysical properties. While in the single crystalline solid state a dominant phosphorescent component from ^{3}LLCT/Cbz states at λ_{max} = 564 (**1**) and 549 (**2**) nm is observed, grinding greatly enhances the efficiency of the TADF process with high k_r of up to $3.1 \cdot 10^5$ s^{-1} and a bathochromic shift of the emitting $^{1/3}$LLCT states to λ_{max} = 579 (**1**) and 606 (**2**) nm. The influence of intermolecular hydrogen bonding on the excited state energies is very relevant for the choice of matrix material for device preparation, as polar and sterically unprotected mCP or PMMA shift the emission hypsochromically into the green region of the electromagnetic spectrum with a drastic decrease of k_r to $< 5 \cdot 10^4$ and $< 0.5 \cdot 10^4$ s^{-1} for **1** and **2**, respectively, while unpolar UGH-3 or bulky CzSi maintain the excellent TADF properties of the copper(I) complexes at lower emission energies. The chirality of the emitter molecules induces a significant rotatory strength of the electronic transitions, resulting in circularly polarized luminescence with excellent dissymmetry factors g_{lum} of $\pm 7 \cdot 10^{-3}$ (**1**) and $\pm 6 \cdot 10^{-3}$ (**2**) in solution, and $\pm 2.3 \cdot 10^{-2}$ for **(*S*)-1/(*R*)-2** in the solid state. Time-resolved CPL measurements reveal that both the T_1 and S_1 state exhibit the same level of rotatory strength. The CPL properties are maintained under electroluminescent conditions, and we demonstrate the application of this class of chiral triplet exciton emitters in proof-of-concept CP-OLEDs with various matrix materials, indicating that careful device design is an important factor for efficient generation of CP electroluminescence.

ASSOCIATED CONTENT

Supporting Information

Experimental details, depiction of further spectra, and DFT calculations.

The Supporting Information is available free of charge on the ACS Publications website.

AUTHOR INFORMATION

Corresponding Author

* andreas.steffen@, jpflaum@physik.uni-wuerzburg.de

Author Contributions

The manuscript was written through contributions of all authors. All authors have given approval to the final version of the manuscript.

ACKNOWLEDGMENT

We thank Prof. G. H. Clever and Dr. J. Tessarolo (TU Dortmund University) for access to a CD and CPL spectrometer and K. Terlinden and Prof. S. Henke for access to a XRPD diffractometer and TGA system. Financial support by the Deutsche Forschungsgemeinschaft (DFG, STE1834/4-2) is gratefully acknowledged. This work was also supported by the DFG Priority Program SPP 2102 "Light-controlled reactivity of metal complexes" (STE1834/7-1) as well as by the Bavarian collaborative research project "Solar Technologies go Hybrid" (SolTech).

REFERENCES

(1) Bennett, C. H.; Brassard, G. Quantum cryptography: Public key distribution and coin tossing. *Theor. Comput. Sci.* **2014**, *560*, 7–11.

(2) Heffern, M. C.; Matosziuk, L. M.; Meade, T. J. Lanthanide probes for bioresponsive imaging. *Chem. Rev.* **2014**, *114* (8), 4496–4539.

(3) Brandt, J. R.; Salerno, F.; Fuchter, M. J. The added value of small-molecule chirality in technological applications. *Nat. Rev. Chem.* **2017**, *1* (6).

(4) Farshchi, R.; Ramsteiner, M.; Herfort, J.; Tahraoui, A.; Grahn, H. T. Optical communication of spin information between light emitting diodes. *Appl. Phys. Lett.* **2011**, *98* (16), 162508.

(5) Wagenknecht, C.; Li, C.-M.; Reingruber, A.; Bao, X.-H.; Goebel, A.; Chen, Y.-A.; Zhang, Q.; Chen, K.; Pan, J.-W. Experimental demonstration of a heralded entanglement source. *Nat. Photon.* **2010**, *4* (8), 549–552.

(6) Fowles, G. R. *Introduction to modern optics*, Second edition, Dover edition; Dover Publications, Inc, 2012.

(7) Kong, F.-F.; Tian, X.-J.; Zhang, Y.; Yu, Y.-J.; Jing, S.-H.; Zhang, Y.; Tian, G.-J.; Luo, Y.; Yang, J.-L.; Dong, Z.-C.; Hou, J. G. Probing intramolecular vibronic coupling through vibronic-state imaging. *Nat. Commun.* **2021**, *12* (1), 1280.

(8) Arrico, L.; Di Bari, L.; Zinna, F. Quantifying the Overall Efficiency of Circularly Polarized Emitters. *Chem. Eur. J.* **2021**, *27* (9), 2920–2934.

(9) Rosenfeld, L. Quantenmechanische Theorie der natürlichen optischen Aktivität von Flüssigkeiten und Gasen. *Z. Physik* **1929**, *52* (3-4), 161–174.

(10) Schellman, J. A. Circular dichroism and optical rotation. *Chem. Rev.* **1975**, *75* (3), 323–331.

(11) Berova, N., Ed. *Circular dichroism*:*Principles and applications*, 2. ed.; Wiley-VCH, 2000.

(12) Meskers, S. C. J. Circular Polarization of Luminescence as a Tool To Study Molecular Dynamical Processes. *ChemPhotoChem* **2022**, *6* (1).

(13) Nagata, Y.; Mori, T. Irreverent Nature of Dissymmetry Factor and Quantum Yield in Circularly Polarized Luminescence of Small Organic Molecules. *Front. Chem.* **2020**, *8*, 448.

(14) Hu, J.-Y.; Ning, Y.; Meng, Y.-S.; Zhang, J.; Wu, Z.-Y.; Gao, S.; Zhang, J.-L. Highly near-IR emissive ytterbium(III) complexes with unprecedented quantum yields. *Chem. Sci.* **2017**, *8* (4), 2702–2709.

(15) Murawski, C.; Leo, K.; Gather, M. C. Efficiency roll-off in organic light-emitting diodes. *Adv. Mater.* **2013**, *25* (47), 6801–6827.

(16) Bünzli, J.-C. G.; Eliseeva, S. V. Basics of Lanthanide Photophysics. In *Lanthanide Luminescence*:*Photophysical, Analytical and Biological Aspects*; Hänninen, P., Härmä, H., Ala-Kleme, T., Eds.; Springer Series on Fluorescence, Vol. 7; Springer-Verlag Berlin Heidelberg, 2011; pp 1–45.

(17) Doistau, B.; Jiménez, J.-R.; Piguet, C. Beyond Chiral Organic (p-Block) Chromophores for Circularly Polarized Luminescence: The Success of d-Block and f-Block Chiral Complexes. *Front. Chem.* **2020**, *8*, 555.

(18) Takaishi, K.; Nakatsuka, Y.; Asano, H.; Yamada, Y.; Ema, T. Ruthenium Complexes Bearing Axially Chiral Bipyridyls: The Mismatched Diastereomer Showed Red Circularly Polarized Phosphorescence. *Chem. Eur. J.* **2022**, *28* (6), e202104212.

(19) Pander, P.; Zaytsev, A. V.; Sil, A.; Williams, J. A. G.; Lanoe, P.-H.; Kozhevnikov, V. N.; Dias, F. B. The role of dinuclearity in promoting thermally activated delayed fluorescence (TADF) in cyclometallated, N^C^N-coordinated platinum(II) complexes. *J. Mater. Chem. C* **2021**, *9* (32), 10276–10287.

(20) Brandt, J. R.; Wang, X.; Yang, Y.; Campbell, A. J.; Fuchter, M. J. Circularly Polarized Phosphorescent Electroluminescence with a High Dissymmetry Factor from PHOLEDs Based on a Platinahelicene. *J. Am. Chem. Soc.* **2016**, *138* (31), 9743–9746.

(21) Park, G.; Kim, H.; Yang, H.; Park, K. R.; Song, I.; Oh, J. H.; Kim, C.; You, Y. Amplified circularly polarized phosphorescence

from co-assemblies of platinum(II) complexes. *Chem. Sci.* **2019**, *10* (5), 1294–1301.
(22) Jiménez, J.-R.; Doistau, B.; Cruz, C. M.; Besnard, C.; Cuerva, J. M.; Campaña, A. G.; Piguet, C. Chiral Molecular Ruby $[Cr(dqp)_2]^{3+}$ with Long-Lived Circularly Polarized Luminescence. *J. Am. Chem. Soc.* **2019**, *141* (33), 13244–13252.
(23) Jiménez, J. ‐ R.; Poncet, M.; Míguez ‐ Lago, S.; Grass, S.; Lacour, J.; Besnard, C.; Cuerva, J. M.; Campaña, A. G.; Piguet, C. Bright Long ‐ Lived Circularly Polarized Luminescence in Chiral Chromium(III) Complexes. *Angew. Chem.* **2021**, *133* (18), 10183–10190.
(24) Dee, C.; Zinna, F.; Kitzmann, W. R.; Pescitelli, G.; Heinze, K.; Di Bari, L.; Seitz, M. Strong circularly polarized luminescence of an octahedral chromium(III) complex. *Chem. Commun.* **2019**, *55* (87), 13078–13081.
(25) Otto, S.; Grabolle, M.; Förster, C.; Kreitner, C.; Resch-Genger, U.; Heinze, K. $[Cr(ddpd)_2]^{3+}$:A Molecular, Water-Soluble, Highly NIR-Emissive Ruby Analogue. *Angew. Chem. Int. Ed.* **2015**, *54* (39), 11572–11576.
(26) Deng, M.; Mukthar, N. F. M.; Schley, N. D.; Ung, G. Yellow Circularly Polarized Luminescence from C_1 -Symmetrical Copper(I) Complexes. *Angew. Chem. Int. Ed.* **2020**, *59* (3), 1228–1231.
(27) Braker, E. E.; Mukthar, N. F. M.; Schley, N. D.; Ung, G. Substituent Effect on the Circularly Polarized Luminescence of C_1 ‐ Symmetric Carbene ‐ Copper(I) Complexes. *ChemPhotoChem* **2021**, *5* (10), 902–905.
(28) Kong, Y.-J.; Yan, Z.-P.; Li, S.; Su, H.-F.; Li, K.; Zheng, Y.-X.; Zang, S.-Q. Photoresponsive Propeller-like Chiral AIE Copper(I) Clusters. *Angew. Chem. Int. Ed.* **2020**, *59* (13), 5336–5340.
(29) Wang, J.-J.; Zhou, H.-T.; Yang, J.-N.; Feng, L.-Z.; Yao, J.-S.; Song, K.-H.; Zhou, M.-M.; Jin, S.; Zhang, G.; Yao, H.-B. Chiral Phosphine-Copper Iodide Hybrid Cluster Assemblies for Circularly Polarized Luminescence. *J. Am. Chem. Soc.* **2021**, *143* (29), 10860–10864.
(30) Yao, L.; Niu, G.; Li, J.; Gao, L.; Luo, X.; Xia, B.; Liu, Y.; Du, P.; Li, D.; Chen, C.; Zheng, Y.; Xiao, Z.; Tang, J. Circularly Polarized Luminescence from Chiral Tetranuclear Copper(I) Iodide Clusters. *J. Phys. Chem. Lett.* **2020**, *11* (4), 1255–1260.
(31) Zhang, M.-Y.; Li, Z.-Y.; Lu, B.; Wang, Y.; Ma, Y.-D.; Zhao, C.-H. Solid-State Emissive Triarylborane-Based [2.2]Paracyclophanes Displaying Circularly Polarized Luminescence and Thermally Activated Delayed Fluorescence. *Org. Lett.* **2018**, *20* (21), 6868–6871.
(32) Sharma, N.; Spuling, E.; Mattern, C. M.; Li, W.; Fuhr, O.; Tsuchiya, Y.; Adachi, C.; Bräse, S.; Samuel, I. D. W.; Zysman-Colman, E. Turn on of sky-blue thermally activated delayed fluorescence and circularly polarized luminescence (CPL) via increased torsion by a bulky carbazolophane donor. *Chem. Sci.* **2019**, *10* (27), 6689–6696.
(33) Li, M.; Wang, Y.-F.; Zhang, D.; Duan, L.; Chen, C.-F. Axially Chiral TADF-Active Enantiomers Designed for Efficient Blue Circularly Polarized Electroluminescence. *Angew. Chem. Int. Ed.* **2020**, *59* (9), 3500–3504.
(34) Roesch, P.; Nitsch, J.; Lutz, M.; Wiecko, J.; Steffen, A.; Müller, C. Synthesis and photoluminescence properties of an unprecedented phosphinine-Cu_4Br_4 cluster. *Inorg. Chem.* **2014**, *53* (18), 9855–9859.
(35) Nitsch, J.; Kleeberg, C.; Fröhlich, R.; Steffen, A. Luminescent copper(I) halide and pseudohalide phenanthroline complexes revisited: simple structures, complicated excited state behavior. *Dalton Trans.* **2015**, *44* (15), 6944–6960.
(36) Bissinger, P.; Steffen, A.; Vargas, A.; Dewhurst, R. D.; Damme, A.; Braunschweig, H. Unexpected luminescence behavior of coinage metal π-diborene complexes. *Angew. Chem. Int. Ed.* **2015**, *54* (14), 4362–4366.
(37) Nitsch, J.; Lacemon, F.; Lorbach, A.; Eichhorn, A.; Cisnetti, F.; Steffen, A. Cuprophilic interactions in highly luminescent dicopper(I)-NHC-picolyl complexes - fast phosphorescence or TADF? *Chem. Commun.* **2016**, *52* (14), 2932–2935.
(38) Hupp, B.; Schiller, C.; Lenczyk, C.; Stanoppi, M.; Edkins, K.; Lorbach, A.; Steffen, A. Synthesis, Structures, and Photophysical Properties of a Series of Rare Near-IR Emitting Copper(I) Complexes. *Inorg. Chem.* **2017**, *56* (15), 8996–9008.
(39) Hobbollahi, E.; List, M.; Hupp, B.; Mohr, F.; Berger, R. J. F.; Steffen, A.; Monkowius, U. Highly efficient cold-white light emission in a $[Au_2CuCl_2(P \cap N)_2]PF_6$ type salt. *Dalton Trans.* **2017**, *46* (11), 3438–3442.
(40) Gernert, M.; Mueller, U.; Haehnel, M.; Pflaum, J.; Steffen, A. A Cyclic Alkyl(amino)carbene as Two-Atom π-Chromophore Leading to the First Phosphorescent Linear Cu^I Complexes. *Chem. Eur. J.* **2017**, *23* (9), 2206–2216.
(41) Braunschweig, H.; Dellermann, T.; Dewhurst, R. D.; Hupp, B.; Kramer, T.; Mattock, J. D.; Mies, J.; Phukan, A. K.; Steffen, A.; Vargas, A. Strongly Phosphorescent Transition Metal π-Complexes of Boron-Boron Triple Bonds. *J. Am. Chem. Soc.* **2017**, *139* (13), 4887–4893.
(42) Hupp, B.; Nitsch, J.; Schmitt, T.; Bertermann, R.; Edkins, K.; Hirsch, F.; Fischer, I.; Auth, M.; Sperlich, A.; Steffen, A. Stimulus-Triggered Formation of an Anion-Cation Exciplex in Copper(I) Complexes as a Mechanism for Mechanochromic Phosphorescence. *Angew. Chem. Int. Ed.* **2018**, *57* (41), 13671–13675.
(43) Liske, A.; Wallbaum, L.; Hölzel, T.; Föller, J.; Gernert, M.; Hupp, B.; Ganter, C.; Marian, C. M.; Steffen, A. Cu–F Interactions between Cationic Linear N-Heterocyclic Carbene Copper(I) Pyridine Complexes and Their Counterions Greatly Enhance Blue Luminescence Efficiency. *Inorg. Chem.* **2019**, *58* (9), 5433–5445.
(44) Gernert, M.; Balles-Wolf, L.; Kerner, F.; Müller, U.; Schmiedel, A.; Holzapfel, M.; Marian, C. M.; Pflaum, J.; Lambert, C.; Steffen, A. Cyclic (Amino)(aryl)carbenes Enter the Field of Chromophore Ligands: Expanded π System Leads to Unusually Deep Red Emitting Cu^I Compounds. *J. Am. Chem. Soc.* **2020**, *142* (19), 8897–8909.
(45) Tzouras, N. V.; Martynova, E. A.; Ma, X.; Scattolin, T.; Hupp, B.; Busen, H.; Saab, M.; Zhang, Z.; Falivene, L.; Pisanò, G.; van Hecke, K.; Cavallo, L.; Cazin, C. S. J.; Steffen, A.; Nolan, S. P. Simple Synthetic Routes to Carbene-M-Amido (M=Cu, Ag, Au) Complexes for Luminescence and Photocatalysis Applications. *Chemistry* **2021**, *27* (46), 11904–11911.
(46) Steffen, A.; Hupp, B. Design of Efficient Emissive Materials. In *Comprehensive Coordination Chemistry III,* 3rd ed.; Constable, E., Ed.; Elsevier, 2021; pp 466–502.
(47) Hölzel, T.; Belyaev, A.; Terzi, M.; Stenzel, L.; Gernert, M.; Marian, C. M.; Steffen, A.; Ganter, C. Linear Carbene Pyridine Copper Complexes with Sterically Demanding *N*,*N*'-Bis(trityl)imidazolylidene: Syntheses, Molecular Structures, and Photophysical Properties. *Inorg. Chem.* **2021**, *60* (23), 18529–18543.
(48) Romanov, A. S.; Jones, S. T. E.; Gu, Q.; Conaghan, P. J.; Drummond, B. H.; Feng, J.; Chotard, F.; Buizza, L.; Foley, M.; Linnolahti, M.; Credgington, D.; Bochmann, M. Carbene metal amide photoemitters: tailoring conformationally flexible amides for full color range emissions including white-emitting OLED. *Chem. Sci.* **2020**, *11* (2), 435–446.
(49) Gu, Q.; Chotard, F.; Eng, J.; Reponen, A.-P. M.; Vitorica-Yrezabal, I. J.; Woodward, A. W.; Penfold, T. J.; Credgington, D.; Bochmann, M.; Romanov, A. S. Excited-State Lifetime Modulation by Twisted and Tilted Molecular Design in Carbene-Metal-Amide Photoemitters. *Chem. Mater.* **2022**.
(50) Titov, A. A.; Filippov, O. A.; Smol'yakov, A. F.; Averin, A. A.; Shubina, E. S. Copper(I) complex with BINAP and 3,5-dimethylpyrazole: synthesis and photoluminescent properties. *Mendeleev Commun.* **2019**, *29* (5), 570–572.
(51) Lotito, K. J.; Peters, J. C. Efficient luminescence from easily prepared three-coordinate copper(I) arylamidophosphines. *Chem. Commun.* **2010**, *46* (21), 3690–3692.
(52) Hattori, G.; Sakata, K.; Matsuzawa, H.; Tanabe, Y.; Miyake, Y.; Nishibayashi, Y. Copper-catalyzed enantioselective propargylic amination of propargylic esters with amines: copper-allenylidene complexes as key intermediates. *J. Am. Chem. Soc.* **2010**, *132* (30), 10592–10608.
(53) El ‐ Sayed, M. A. Spin−Orbit Coupling and the Radiationless Processes in Nitrogen Heterocyclics. *J. Chem. Phys.* **1963**, *38* (12), 2834–2838.

(54) Siebrand, W. Radiationless Transitions in Polyatomic Molecules. II. Triplet ‐ Ground ‐ State Transitions in Aromatic Hydrocarbons. *J. Chem. Phys.* **1967**, *47* (7), 2411–2422.
(55) Siebrand, W. Radiationless Transitions in Polyatomic Molecules. I. Calculation of Franck—Condon Factors. *J. Chem. Phys.* **1967**, *46* (2), 440–447.
(56) Englman, R.; Jortner, J. The energy gap law for radiationless transitions in large molecules. *Mol. Phys.* **1970**, *18* (2), 145–164.
(57) Hamze, R.; Peltier, J. L.; Sylvinson, D.; Jung, M.; Cardenas, J.; Haiges, R.; Soleilhavoup, M.; Jazzar, R.; Djurovich, P. I.; Bertrand, G.; Thompson, M. E. Eliminating nonradiative decay in Cu(I) emitters: 99% quantum efficiency and microsecond lifetime. *Science* **2019**, *363* (6427), 601–606.
(58) Föller, J.; Marian, C. M. Rotationally Assisted Spin-State Inversion in Carbene-Metal-Amides Is an Artifact. *J. Phys. Chem. Lett.* **2017**, *8* (22), 5643–5647.
(59) Bylina, A. Triplet-Triplet energy transfer and the overlap of singlet-triplet bands of sensitizer and acceptor. Remarks on the 'phantom triplet' of stilbene. *Chem. Phys. Lett.* **1968**, *1* (11), 509–510.
(60) Feng, J.; Taffet, E. J.; Reponen, A.-P. M.; Romanov, A. S.; Olivier, Y.; Lemaur, V.; Yang, L.; Linnolahti, M.; Bochmann, M.; Beljonne, D.; Credgington, D. Carbene–Metal–Amide Polycrystalline Materials Feature Blue Shifted Energy yet Unchanged Kinetics of Emission. *Chem. Mater.* **2020**, *32* (11), 4743–4753.
(61) Ruduss, A.; Turovska, B.; Belyakov, S.; Stucere, K. A.; Vembris, A.; Baryshnikov, G.; Ågren, H.; Lu, J.-C.; Lin, W.-H.; Chang, C.-H.; Traskovskis, K. Thiazoline Carbene-Cu(I)-Amide complexes: Efficient White Electroluminescence from Combined Monomer and Excimer Emission. *ACS Appl. Mater. Interfaces* **2022**, *14* (13), 15478–15493.
(62) Lüdtke, N.; Föller, J.; Marian, C. M. Understanding the luminescence properties of Cu(I) complexes: a quantum chemical perusal. *Phys. Chem. Chem. Phys.* **2020**, *22* (41), 23530–23544.
(63) Stefan C. J. Meskers; Harry P. J. M. Dekkers; Gwénaël Rapenne; Jean-Pierre Sauvage. Chiroptical Properties of an Optically Pure Dicopper(I) Trefoil Knot and Its Enantioselectivity in Luminescence Quenching Reactions. *Chem. Eur. J.* **2000**, *6* (12), 2129–2134.
(64) Song, J.; Xiao, H.; Fang, L.; Qu, L.; Zhou, X.; Xu, Z.-X.; Yang, C.; Xiang, H. Highly Phosphorescent Planar Chirality by Bridging Two Square-Planar Platinum(II) Complexes: Chirality Induction and Circularly Polarized Luminescence. *J. Am. Chem. Soc.* **2022**, *144* (5), 2233–2244.
(65) Zinna, F.; Pasini, M.; Galeotti, F.; Botta, C.; Di Bari, L.; Giovanella, U. Design of Lanthanide-Based OLEDs with Remarkable Circularly Polarized Electroluminescence. *Adv. Funct. Mater.* **2017**, *27* (1), 1603719.
(66) Peeters, E.; Christiaans, M. P. T.; Janssen, R. A. J.; Schoo, H. F. M.; Dekkers, H. P. J. M.; Meijer, E. W. Circularly Polarized Electroluminescence from a Polymer Light-Emitting Diode. *J. Am. Chem. Soc.* **1997**, *119* (41), 9909–9910.
(67) Zinna, F.; Giovanella, U.; Di Bari, L. Highly circularly polarized electroluminescence from a chiral europium complex. *Adv. Mater.* **2015**, *27* (10), 1791–1795.

Enantiomerically pure chiral copper(I) BINAP complexes show efficient thermally activated delayed fluorescence (TADF) with mechano-stimulus behavior due to specific C-H···π interactions of the ligands with the environment, that can be disrupted by grinding. The high dissymmetry factors g_{lum} for circular polarized luminescence (CPL) of up to $2.3 \cdot 10^{-2}$ lead to application of the copper(I) emitters in proof-of-concept CPL-OLEDs.